DFT-based Polarizable Ion Models for Molten Rare-earth Chlorides: from Lanthanum to Europium

Kateryna Goloviznina,[†] Maria-Chiara Notarangelo,[‡] Julien Tranchida,[‡] Emeric Bourasseau,[‡] and Mathieu Salanne[*,†,¶]

†*Sorbonne Université, CNRS, Physicochimie des Électrolytes et Nanosystèmes Interfaciaux, F-75005 Paris, France*

‡*DES, IRESNE, DEC, CEA Cadarache, Saint-Paul-Lez-Durance 13108, France*

¶*Institut Universitaire de France (IUF), 75231 Paris, France*

E-mail: mathieu.salanne@sorbonne-universite.fr

Abstract

We developed a systematic polarizable force field for molten trivalent rare-earth chlorides, from lanthanum to europium, based on first-principle calculations. The proposed model was employed to investigate the local structure and physico-chemical properties of pure molten salts and their mixtures with sodium chloride. We computed densities, heat capacities, surface tensions, viscosities and diffusion coefficients and disclosed their evolution along the lanthanide series, filling the gaps for poorly studied elements, such as promethium and europium. The analysis of the local arrangement of chloride anions around lanthanide cations revealed broad coordination number distributions with a typical [from six to nine]-fold environment, the maximum of which shifts towards lower values with the increase of atomic number as well as upon dilution of the salt in sodium chloride. The neighbouring lanthanide-chloride complexes were found to be connected by sharing a corner or an edge of the corresponding polyhedra.

Introduction

Nowadays, molten salts are considered to be a promising fuel for the nuclear reactors of the fourth generation, such as molten chloride fast reactors (MCFRs).[1,2] Primarily composed of fissile and fertile actinide chlorides mixed with alkali and alkaline earth metal salts, they serve as a good alternative to traditional metal-oxide systems because of their liquid state and nearly atmospheric operating pressures, which notably reduces the risk of accidents.[3,4]

In such fuels, many rare-earth elements are accumulated as fission products during the operation of the reactor and can be further separated using electrolysis.[5,6] Moreover, some of them are commonly used as analogues to actinides (La for U and Ce for Pu) when investigating experimentally the physico-chemical properties of such fuels and the nuclear recycling treatment.[7–10] Therefore, it is crucial to fully understand the behaviour of lanthanide salts in such melts, in particular, the features of the local arrangement and their impact on the system properties. The structural information such as coordination numbers is commonly used

in analytical models to develop thermodynamic databases[11,12] for multi-component molten salt systems.

An important question, widely discussed in the literature, is how rare-earth ions are coordinated in different environments. For example, high coordination numbers are known for lanthanide solvated by aqueous and non-aqueous solvents. Using classical molecular dynamics (MD) simulations, Spezia *et al.*[13,14] demonstrated 8–9-fold geometries for $[M(H_2O)_n]^{3+}$ complexes, with M^{3+} ranging from La^{3+} to Lu^{3+}. The coordination numbers as well as the most probable cation-water distance decreased along the series, which was explained by the change in the ionic radii. These observations were confirmed by X-ray absorption spectroscopy (XAS) techniques and Density Functional Theory (DFT) calculations.[15] Similar coordination numbers were also reported for solutions of MCl_3 in DMSO.[16,17]

Nevertheless, the discussion on lanthanide coordination in pure molten salt is more ambiguous. Based on Raman spectra, some earlier works[18,19] claimed a solitary octahedral coordination of the La^{3+} cation. Currently, the scientific community[8,20] tends to believe that La^{3+} cation can adopt a variety of $LaCl_n^{(n-3)-}$ coordinations, with n reaching 6–9, as was proposed by Madden and co-workers based on polarisable MD simulations.[21,22] Considering the $LaCl_3$ salt, these authors demonstrated that the presence of complexes with $n > 6$ does not lead to any new features in the computed Raman spectra compared to $[LaCl_6]^{3-}$, yielding a good agreement between simulated and measured data. The broad coordination number distribution was confirmed by several experimental techniques, including X-ray absorption fine structure (XAFS),[23,24] and x-ray diffraction,[25] coupled with MD simulations.

As was shown before, classical MD simulations play an indispensable role in interpreting the experimental results and identifying structure-property relationships. The presence of explicit polarisation effects is essential to provide a reliable description of molten halide salts, which contain highly polarising and polarisable ions.[26] The most rigorous approach proposed in the literature is the polarisable ion model (PIM) by Madden and co-workers,[27,28] which is already available for families of monovalent[29] and bivalent[30] cations. Studies of the trivalent

cations, typically considered as mixtures with alkali halide melt, are mainly focused on La^{3+}, Sc^{3+}, Y^{3+} and U^{3+},[31,32] with only a few isolated publications going further to Ce^{3+},[33] Nd^{3+},[34] Sm^{3+}[35]. In a recent work, *ab-initio* MD simulations were also used to simulate the properties of a series of lanthanides in the LiCl-KCl eutectic melt.[36,37] However, the literature lacks a systematic investigation of the trivalent lanthanide cations by means of classical MD simulations, first of all, because of the absence of a general polarisable model, and this gap we aim to fill in.

In the present work, we will propose a transferable polarisable force field for trivalent cations for the first half of the lanthanide series, from La^{3+} to Eu^{3+}, combined with chloride anion, developed on first-principle calculations. We will reveal the systematic trends in the evolution of local arrangement and transport properties in pure melts along the series, shedding light on the coordination environment and diffusivity trends. The discussion will be then extended to the MCl_3/NaCl mixtures with low (1 % by molar fraction) lanthanide salt content in order to mimic more realistic experimental conditions for nuclear applications.

Methods

Force field development

In the PIM model,[27,28] the total potential energy consists of the Coulomb, polarization and Born-Mayer potentials,

$$\phi^{\mathrm{tot}} = \phi^{\mathrm{Coul}} + \phi^{\mathrm{pol}} + \phi^{\mathrm{BM}}. \tag{1}$$

The Born-Mayer potential accounts for repulsion and dispersion terms,

$$\phi^{\mathrm{BM}} = B_{ij}\exp(-\alpha_{ij}r_{ij}) - \\ - \sum_i \sum_{j>i} \left(\frac{C_6^{ij}}{r_{ij}^6} f_6^{ij}(r_{ij}) + \frac{C_8^{ij}}{r_{ij}^8} f_8^{ij}(r_{ij}) \right), \tag{2}$$

with r_{ij} the distance between two ions labeled i and j, α_{ij}, B_{ij}, C_6^{ij}, and C_8^{ij} constant coefficients depending on the respective species of atoms i and j. The polarisation energy includes charge-dipole, dipole-dipole, and self-interaction contributions,

$$\phi^{\mathrm{pol}} = \sum_i \sum_{j>i} \left(\frac{q_i \boldsymbol{r}_{ij} \cdot \boldsymbol{\mu}_j}{r_{ij}^3} f_4^{ij}(r_{ij}) + \frac{\boldsymbol{\mu}_i \cdot q_j \boldsymbol{r}_{ji}}{r_{ij}^3} f_4^{ji}(r_{ij}) \right) + \\ + \sum_i \sum_{j>i} \left(\frac{\boldsymbol{\mu}_i \cdot \boldsymbol{\mu}_j}{r_{ij}^3} + \frac{3(\boldsymbol{\mu}_i \cdot \boldsymbol{r}_{ji})(\boldsymbol{r}_{ij} \cdot \boldsymbol{\mu}_j)}{r_{ij}^5} \right) + \\ + \sum_i \frac{|\boldsymbol{\mu}_i|^2}{2\alpha_i}, \quad (3)$$

with q_i and μ_i the charge and dipole moment associated to an ion i, respectively. In both equation 2 and 3, $f_n^{ij}(r_{ij})$ refers to Tang-Toennies damping functions, applied to the dispersive and charge-dipole interactions[38], given by:

$$f_n^{ij}(r_{ij}) = 1 - c_n^{ij} \exp(-b_n^{ij} r_{ij}) \sum_{k=0}^{n} \frac{(b_n^{ij} r_{ij})^k}{k!}. \quad (4)$$

Table 1: Atomic polarisabilities for molten salt ions. The values for Na^+ and Cl^- species were taken from reference 29.

Ion	Polarisability
La^{3+}	8.445
Ce^{3+}	7.874
Pr^{3+}	7.790
Nd^{3+}	6.619
Pm^{3+}	6.276
Sm^{3+}	6.130
Eu^{3+}	5.828
Na^+	0.900
Cl^-	20.000

All the values are given in atomic units.

The atomic polarisabilities α_i (Table 1, Figure 1a) and repulsion parameter B_{ij} (Table 2, Figure 1b) were obtained through a fitting procedure, during which the deviations in forces

(χ_F^2) between classical MD and DFT data were minimized for a series of given liquid configurations. Four independent liquid configurations containing 62 MCl_3 units in a box with $L \approx 21$ Å were generated by a classical MD run using a $LaCl_3$ force field from our previous study.[31] The target function was defined as

$$\chi_F^2 = \frac{1}{N} \sum^{N} \frac{|\boldsymbol{F}_i^{\mathrm{DFT}} - \boldsymbol{F}_i^{\mathrm{PIM}}|^2}{|\boldsymbol{F}_i^{\mathrm{DFT}}|^2}. \tag{5}$$

The DFT computations were performed with the CP2K[39] software using the Quickstep algorithm.[40] Wave functions were constructed using a basis set of double and triple-ζ quality with DZVP (for lanthanide cations)[41] and TZV2PX (for chloride anions) polarization functions. A 800 Ry plane wave density cutoff was used. All atoms were described using Goedecker–Teter–Hutter (GTH)-type pseudopotentials with Perdew–Burke–Ernzerhof (PBE)[42] as an exchange-correlation functional.

After fitting atomic polarisabilities and repulsion parameters, the dispersion parameters were empirically adjusted. Thus, the individual $C_{6,8}^{ii}$ values for lanthanide metal cations were computed starting from those of La^{3+} (taken from our previous study[31]) and scaled by the atomic polarisability ratio as:

$$C_{6,8}^{ii}(\mathrm{M}^{3+}) = C_{6,8}^{ii}(\mathrm{La}^{3+}) \frac{\alpha(\mathrm{M}^{3+})}{\alpha(\mathrm{La}^{3+})}. \tag{6}$$

The mixed $C_{6,8}^{ij}$ dispersion coefficients for the interaction of lanthanide metal ions with chloride anions or sodium cations were then evaluated using the geometric mixing rule,

$$C_{6,8}^{ij}(\mathrm{M}^{3+}...\mathrm{Cl}^{-}) = \sqrt{C_{6,8}^{ii}(\mathrm{M}^{3+}) \cdot C_{6,8}^{jj}(\mathrm{Cl}^{-})} \tag{7}$$

The resulting dispersion coefficients are provided in Table 2.

The Tang-Toennies damping parameters applied to the charge-dipole interaction were kept constant along the lanthanide series, and the values are given in Table 3.

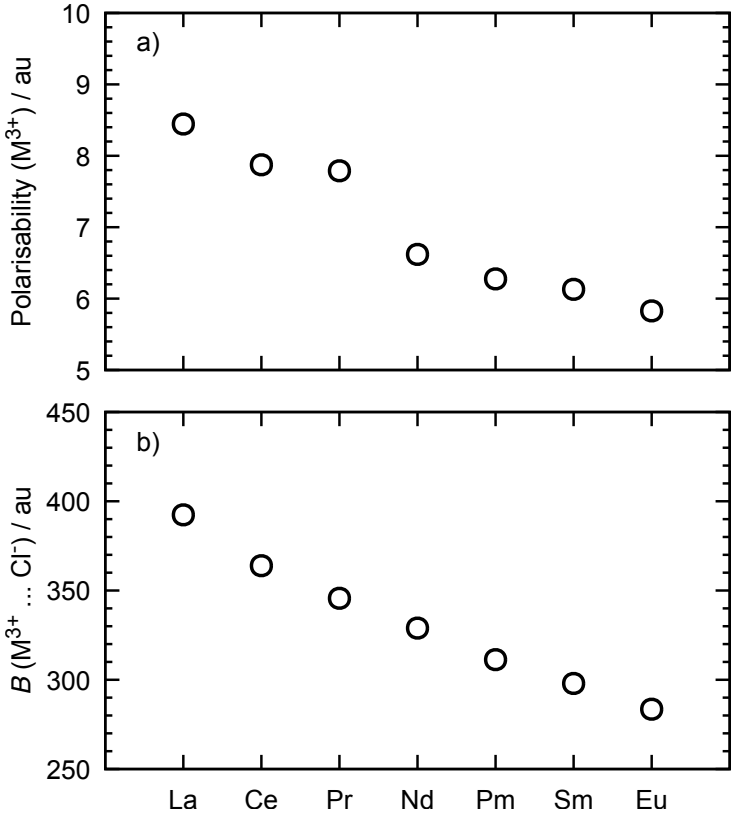

Figure 1: Fitted atomic polarisabilities of metal M^{3+} ions (a) and B^{ij} Born-Mayer repulsion parameter for the $M^{3+}\cdots Cl^-$ interactions (b).

Our force field parameters successfully capture the contraction effect, as well as the decrease of ionic radii with the increase in atomic number, known for lanthanide series, and which impacts their physical and chemical properties.[43,44] Due to a rather diffuse character, the $4f$ orbitals are unable to properly shield the valence $5s$ and $6s$ orbitals resulting in their closer location to the nucleus. Even though we do not have an explicit representation of the electrons, the compression of the electronic cloud is reflected in smaller atomic polarisability values as illustrated by Figure 1a. In addition to this, we capture the diminishing of the ionic radii itself, as a decrease of the prefactor B^{ij} in Born-Mayer repulsion potential for the $M^{3+}\cdots Cl^{-}$ interactions along the series, shown in Figure 1b.

Simulation details

Molecular dynamics simulations were performed using the MetalWalls software[45,46]. The 3D periodic simulation boxes of pure lanthanide chlorides consisted of 500 MCl_3 units, corresponding to a total number of 2000 ions, and were prepared using the PACKMOL[47] utility. The systems were equilibrated for 0.5 ns in the NPT ensemble at 1100 K, 1150 K, 1200 K and 1300 K and 1 bar with a timestep of 1 fs. Then, production runs were performed for 2.0 ns in the NPT ensemble and for 5.0 ns in the NVT ensemble at 1100 K, except for the $LaCl_3$, for which 1150 K was used instead because of its higher melting point. A Nosé–Hoover-chain thermostat was used for temperature control. A cut-off of 10.6 Å was considered for nonbonded interactions, and a tail correction was applied for energy and pressure for bulk simulations. Long-range electrostatic interactions were computed using the Ewald summation method with a tolerance of 10^{-7}.

The simulation boxes containing MCl_3/NaCl mixtures consisted of 7 MCl_3 units and 693 ion pairs of NaCl (1414 atoms in total), which corresponded to composition to 1 % of MCl_3 content (by molar fraction). The systems were equilibrated for 0.5 ns in the NPT ensemble at 1100 K and 1 bar, followed by production runs of 5.0 ns in the NVT ensemble. All other simulation parameters were kept unchanged. Three independent trajectories were considered

for transport property analysis.

Radial distribution functions and coordination numbers were computed using the TRAVIS software,[48,49] and self-written tools.

Viscosities of pure lanthanide salts were evaluated using Green-Kubo approach from the stress tensor autocorrelation functions (ACFs),

$$\eta = \frac{V}{k_{\mathrm{B}}T}\int_0^\infty \langle s_{ij}(t)s_{ij}(0)\rangle dt, \quad ij = xy,\ xz,\ yz. \tag{8}$$

Nevertheless, the ACF suffers from poor convergence, leading to large uncertainties during integration. In order to overcome this issue, we applied the cepstral approach by Baroni *et al.*,[50] available in the SporTran utility.[51] According to this method, the logarithm of the ACF power spectrum in the low-frequency domain (defined by a cutoff Nyqvist frequency of 15 THz) is fitted by a series of cepstral coefficients. This allows for the elimination of noise effects and provides a reliable estimation of dynamics properties from rather short simulation trajectories.

Diffusion coefficients were evaluated from mean-squared displacements using the Einstein's relation,

$$D = \lim_{x\to\infty} \frac{1}{6}\frac{d}{dt}\left\langle (\mathbf{r}(t) - \mathbf{r}(0))^2 \right\rangle \tag{9}$$

and the Yeh-Hummer correction[52,53] was applied to account for finite-size effects,

$$D_0 = D + \frac{2.8373 k_B T}{6\pi\eta L}, \tag{10}$$

The calculated viscosities were used to evaluate the correcting term for the pure lanthanide chlorides. In the case of MCl_3/NaCl mixtures, due to low MCl_3 content, the viscosity value was considered as that of pure NaCl, available in the literature.[54]

To compute the surface tension of neat lanthanide chlorides, separate simulation boxes were prepared starting from the equilibrated bulk configurations. For this, the system was

extended by L in $-z$ and $+z$ directions to create two liquid-vacuum interfaces, resulting in a $L \times L \times 3L$ box, where L is the box side length of the previously equilibrated cubic cell. Then, it was equilibrated for 1.0 ns in the NVT ensemble, followed by a 5.0 ns production run. The 3D periodicity with a slab correction was applied.[55] The surface tension was computed using the Irving-Kirkwood method[56,57] from pressure tensor components p_{xx}, p_{yy} and p_{zz} as

$$\gamma = \frac{L_z}{2}\left(\langle (p_{xx} + p_{yy})/2 \rangle - \langle p_{zz} \rangle\right) \tag{11}$$

The resulting trajectory was divided into 5 equal sub-trajectories of 1.0 ns each, from which the average surface tension value and the standard deviation were evaluated.

Validation

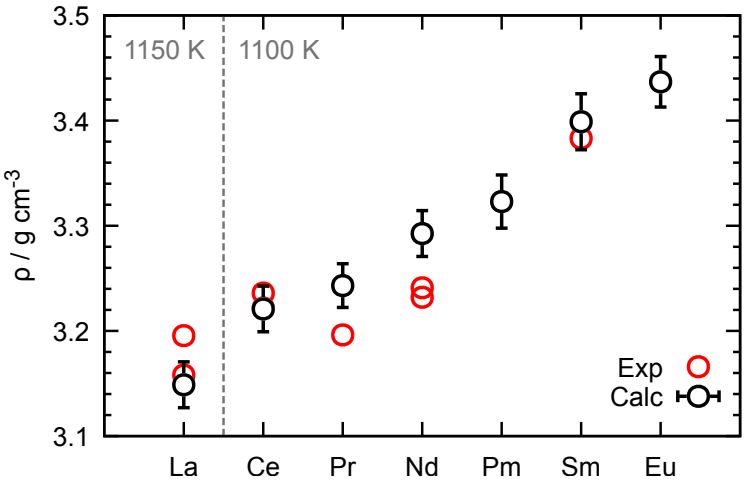

Figure 2: Calculated and experimental[43,54] densities of molten MCl_3 salts. The values are computed at 1100 K for the Ce−Eu systems and at 1150 K for the La system.

Although the dispersion coefficients generally do not impact the structure of molten salts, they have an important effect on the densities of the melts.[28] Therefore, to validate our approach of deriving them from atomic polarisability ratios, we primarily compared the computed densities with the experimental values.[43,54] As shown in Figure 2, the contraction

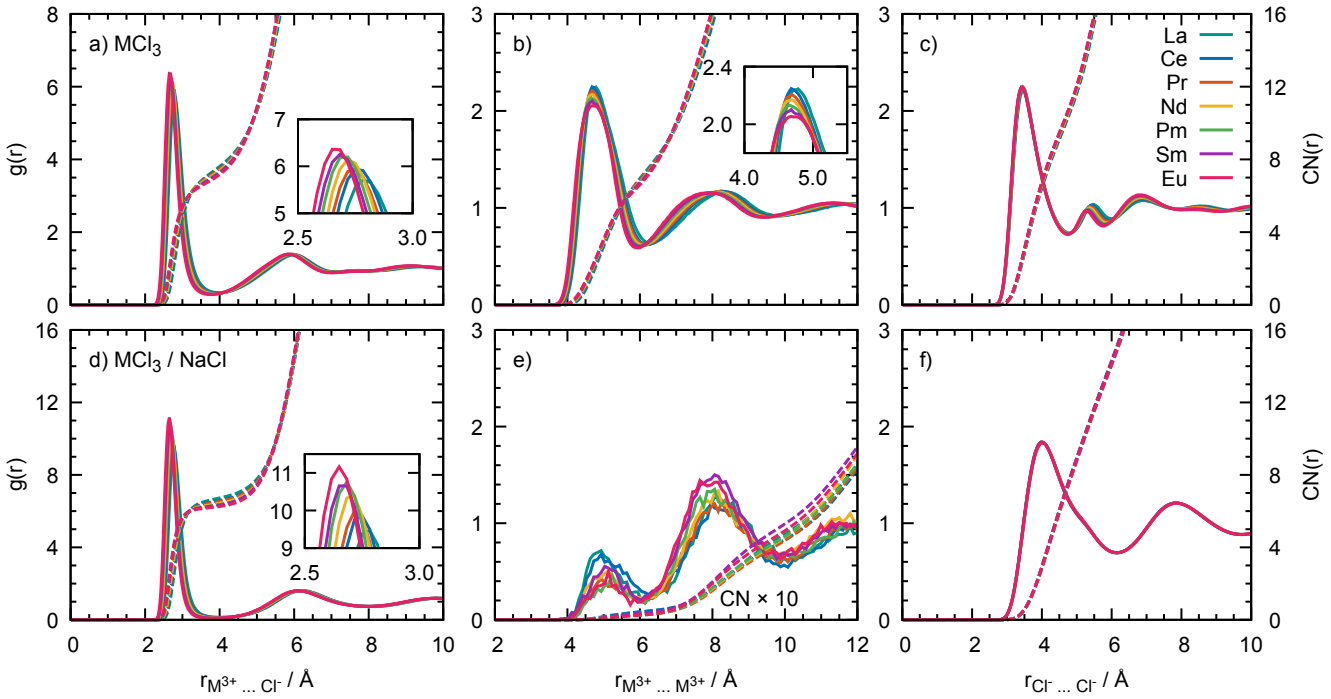

Figure 3: Radial distribution function (g(r), solid lines) and running coordination numbers (CN(r), dashed lines) of the $M^{3+}\cdots Cl^{-}$ (a,d), $M^{3+}\cdots M^{3+}$ (b,e), and $Cl^{-}\cdots Cl^{-}$ (c,f) interactions in neat MCl_3 (a-c) and 1 % MCl_3/NaCl (d-f) systems. The insets show the zoom of the first maximum of the corresponding RDFs.

effect notably impacts the densities of lanthanide chloride melts. The values increase from 3.15–3.25 g mol^{-1} for lanthanum and cerium chlorides up to 3.40–3.45 g mol^{-1} for samarium and europium. We observe a good agreement between two sets of data for $LaCl_3 - NdCl_3$ and $SmCl_3$, with the relative error not exceeding ± 1.8 %. Such small deviations then allow a reliable prediction of densities also for $PmCl_3$ and $EuCl_3$, not available in the literature due to zero natural abundance of Pm metal[58] and thermal decomposition of $EuCl_3$ during melting.[59]

In addition to this, we estimated heat capacity and surface tension values. The heat capacity does not vary much along the series, remaining about 138.4 ± 1.4 J mol^{-1} K^{-1}, as illustrated by Figure S1. The experimental values are rather scattered, being in the range of 126–180 J mol^{-1} K^{-1} [60,61]. The surface tension of a neat salt is approximately 100 mN m^{-1} at 1100–1150 K (Figure S2), while the experimental values vary from 87 to 120 mN m^{-1}.[62–65] Both property values are consistent with the previously reported data, demonstrating relatively small uncertainties, being less scattered and more systematic.

Results

Local structure

The local structure of lanthanide chlorides can be characterised by a set of radial distribution functions (RDFs) for $M^{3+}\cdots Cl^-$, $M^{3+}\cdots M^{3+}$ and $Cl^-\cdots Cl^-$ interactions. As given in Figure 3a, the most probable $M^{3+}\cdots Cl^-$ distance shifts from 2.78 Å for La^{3+} to 2.65 Å for Eu^{3+}, and intensities increase along the series. The obtained separations agree well with the earlier x-ray and neutron diffraction studies.[8,66] The second peak is observed at 6.02 Å for La^{3+}, decreasing to 5.85 Å for Eu^{3+}. Both trends are direct consequences of the lanthanide ionic radius contractions.

The size of the first chloride coordination shell around a lanthanide ion decreases from 4.02 Å for La^{3+} to 3.72 Å for Eu^{3+}, and the average number of anions drops from 7.64 to 6.79.

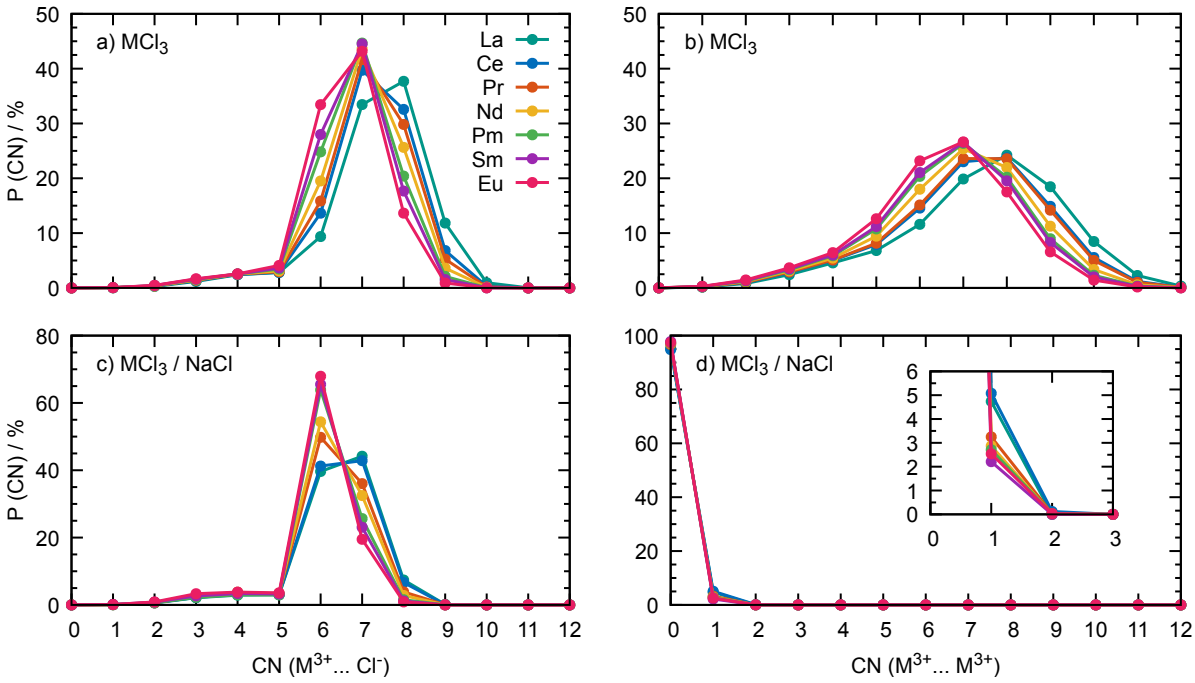

Figure 4: Probabilities of finding a specific number of Cl^- (a,c) and M^{3+} (b,d) atoms in the first M^{3+} coordination shell of molten MCl_3 (a,b) and 1 % MCl_3/NaCl (c,d) systems.

As can be seen from Figure 4a, this is primarily caused by a notable decrease of the CN = 8 fraction from 38 % to 14 % and a corresponding increase of CN = 6 fraction from 10 % to 33 % along the series. The contribution of CN = 7, which is the dominant for Ce^{3+} – Sm^{3+} ions, remains constant, being approximately 40–43 %. The only exception is the La^{3+} ion, for which this contribution is about 33 %, being smaller by several percents than that of CN = 8. These discrepancies between La^{3+} and the rest of the series might be related to a different simulation temperature used for $LaCl_3$ since lanthanide coordination numbers are known to be sensitive to the temperature.[20]

The obtained results agree well with the works of Madden and co-workers[21,22] who based on MD simulations reported a broad $La^{3+}\cdots Cl^-$ coordination number distribution, from 6 to 9, with the predominance of 7 and 8 contributions.[23,24] Average coordination numbers greater than six were also obtained experimentally for molten $CeCl_3$,[67] $NdCl_3$,[68] $EuCl_3$.[69]

The variation of the position of the first $M^{3+}\cdots M^{3+}$ peak is less pronounced, shifting

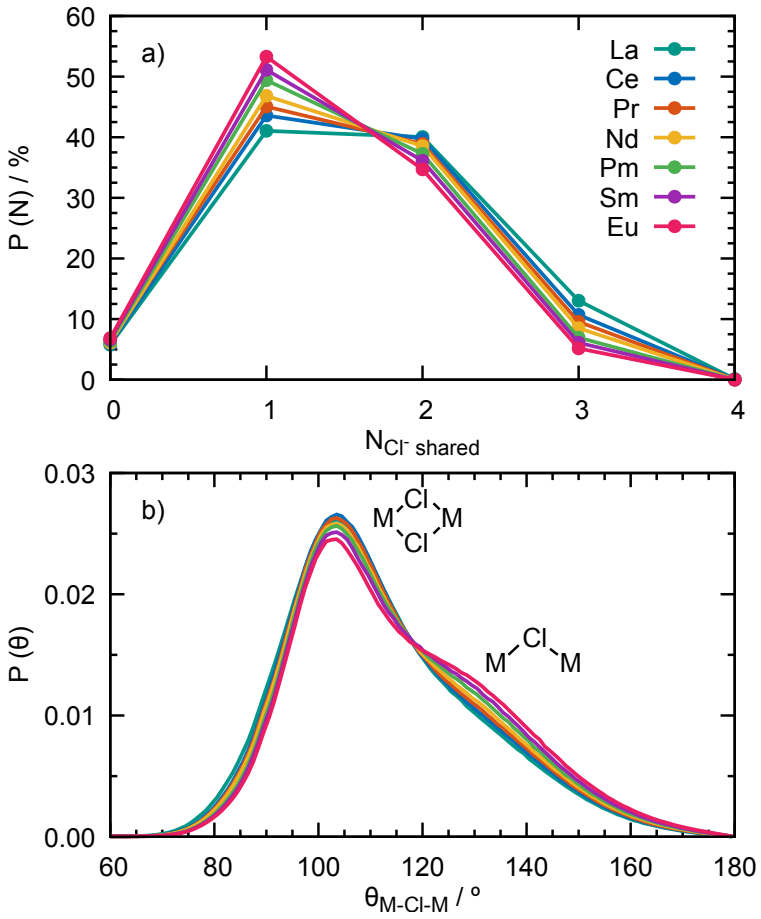

Figure 5: (a) Probabilities of sharing a specific number of Cl^- anion between two neighbouring M^{3+} cations in molten MCl_3 salts. (b) Normalised $M^{3+}\cdots Cl^-\cdots M^{3+}$ angular distribution functions for pairs of M^{3+} cations sharing Cl^- anions in molten MCl_3 salts.

from 4.78 Å for La^{3+} to 4.68 Å for Eu^{3+}, with a small decrease of intensity (Figure 3b). Two neighbouring metal cations share one or two chloride anions, connecting two $MCl_n^{(n-3)-}$ polyhedra through a corner or an edge (Figure 5a). Rarely, in about 5–13 % cases, three chloride anions are shared, so that neighbouring polyhedra share a face. Such a connection between neighbouring polyhedra explains high $M^{3+}\cdots Cl^-$ coordination numbers in molten salt melts.[32] As shown in angular distribution function (ADF) in Figure 5b, the most probable $M^{3+}\cdots Cl^-\cdots M^{3+}$ angle is about 103° with a notable shoulder at about 130–140°. These are peaks corresponding to the $M^{3+}\cdots M^{3+}$ pairs sharing two and one chloride anions, respectively, as shown in the ADF decomposition in Figure S3. The intensity of the dominant ADF peak slightly decreases along the series, while more pronounced changes can be noticed for the shoulder. These observations correlate with the change in the probability of sharing two or one anions, as illustrated by Figure 5a. The position of the peak and the shoulder, however, remain close to constant, explaining why almost no change is observed for the first $M^{3+}\cdots M^{3+}$ RDF maxima (Figure 3b). But the difference in the corner/edge-sharing ratio can be noticed as a change in the intensity of this RDF peak, as discussed in the literature.[32,70]

Similarly to $M^{3+}\cdots Cl^-$ case, the radius of first $M^{3+}\cdots M^{3+}$ coordination shell also decreases by roughly 0.3 Å, from 6.28 Å for La^{3+} to 5.95 Å for Eu^{3+}, while the average coordination number reduces from 7.65 to 6.50. While there are about 7–9 La^{3+} ions around a single La^{3+}, there are just 6–8 cation around a Eu^{3+} as illustrated by Figure 4b. The coordination number distributions are much broader than for those of $M^{3+}\cdots Cl^-$, with the maximum probability for a given value not exceeding 30 %.

The second $M^{3+}\cdots M^{3+}$ peak drastically changes along the series, dropping from 8.35 Å for La^{3+} to 7.88 Å for Eu^{3+}. It is linked to the different packing of the melts and do not correspond to a particular structural feature. Such a change in peak position results from the reorganisation of the connecting pattern between polyhedra, so that the almost equal (≈40 %) probability of sharing one or two chloride anions by La^{3+} ions transforms into the

prevailing of one anion sharing for Eu^{3+} ions (53 % for one Cl^- vs 34 % for two Cl^- as given in Figure 5a).

The most probable distance for the $Cl^- \cdots Cl^-$ pair is observed at about 3.4 Å, with the identical shape of the peak, as shown in Figure 3c. Since there are no changes in the shape and position of the first peak, the size of the first coordination shell also remains constant, of about 4.8 Å. The coordination number does not vary either, fluctuating between 10.5–10.7. The second and third peaks, however, are different along the series, varying from 5.48 Å and 6.95 Å for La^{3+} to 5.28 Å and 6.85 Å for Eu^{3+}, respectively, being a result of the lanthanide ionic radii contraction effect and the network reorganisation.

Obviously, in neat molten lanthanide chloride salts, all metal ions are connected by chloride anions forming one large network.[21] In real industrial mixtures, such as spent nuclear fuels during their reprocessing, the lanthanide concentrations rarely exceed few percents.[71] Therefore, to explore the behaviour of lanthanide ions diluted in another molten salt, we then considered 1 mol % MCl_3/NaCl systems.

The shape of the $M^{3+} \cdots Cl^-$ RDFs in the MCl_3/NaCl systems appear to be quite similar to those in neat MCl_3 as can be seen from the comparison of Figures 3a and 3d. The intensity of the first peak is notably higher, being a signature of a so-called dilution effect, while its position shifts towards smaller values. For the mixtures, the coordination numbers are smaller than for the neat salts, ranging from 6.73 for La^{3+} to 6.22 for Eu^{3+}. A decrease of the coordination numbers with a decrease of the concentration was earlier demonstrated by Madden *et al.*,[21,24] who suggested that the average number of Cl^- anions around a La^{3+} cation approaches 6–6.5 in diluted alkali chloride melts, which also results in a small ($<$ 0.1 Å) diminution of the most probable $M^{3+} \cdots Cl^-$ distance. From the coordination number distributions, shown in Figure 4c, we can see that the dominant values are 7 and 6 for La^{3+}, and their ratio drastically decreases along the series, so that a Eu^{3+} is coordinated by 6 anions in about 73 % of the cases. This trend is consistent with what we observed in neat MCl_3 salts, where the coordination number diminishes with the increase of atomic number.

The $M^{3+}\cdots M^{3+}$ RDF reveals a fingerprint of possible lanthanide metal ion association in the NaCl melt (Figure 3e). The first low-intense peak, corresponding to two metal ions sharing chloride anions, is observed at about 4.9–5.1 Å, slightly at a larger distance than neat MCl_3 salt. The intensities for La^{3+} and Ce^{3+} are higher than for the other cations, indicating that these species have a slightly higher tendency to cluster compared to other species in the series. Nevertheless, for all the lanthanide ions this clustering probability remains low, since 95–98 % of metal ions remain isolated as shown in Figure 4d. The second $M^{3+}\cdots M^{3+}$ peak emerges at about 8.0 Å and is shifted towards lower separation along the series. However, the origin of this peak is different from the pure salt, corresponding to two lanthanide cations separated by a sodium ion. The role of Na^+ cation as a spacer, which disrupts lanthanide network, was suggested by Emmerson *et al.*[20,72] based on x-ray diffraction experiments and classical MD simulations. In their works, the authors demonstrated that the prepeak in the $LaCl_3 - NaCl$ scattering spectrum at about 1 $Å^{-1}$, the origin of which was under discussion for a long time,[73,74] should be attributed to the alternation between the multivalent cations and the spacer salt.

Finally, since the concentration of the lanthanide salt is small, the $Cl^-\cdots Cl^-$ RDF in Figure 3f shows no influence of the lanthanide salt type, being almost identical to that of neat NaCl.

Transport properties

Among several dynamic properties considered in this manuscript, viscosity is the one difficult to compute. Estimated using the Green-Kubo approach, the ACF integrals suffer from convergence issues, even though a recently reported Cepstral analysis method[50] was used to eliminate long-time noise. Presented in Figure 6, the computed values deviate not more than for 25 % from the reported ones by Potapov *et al.*[75] Still, the simulations are unable to capture the experimental trend observed along the series. Here, we should underline that the experimental values are also not straightforward to obtain because of the challenging

high-temperature measurements, difficult preparation procedures and possible presence of impurities. Thus, Potapov *et al.*[75] directly measured the values for $LaCl_3 - NdCl_3$ and $SmCl_3$, and estimated for $PmCl_3$ and $EuCl_3$. We also provide a comparison with other data, available in the literature,[64,76,77] but extrapolated to our simulation temperatures.

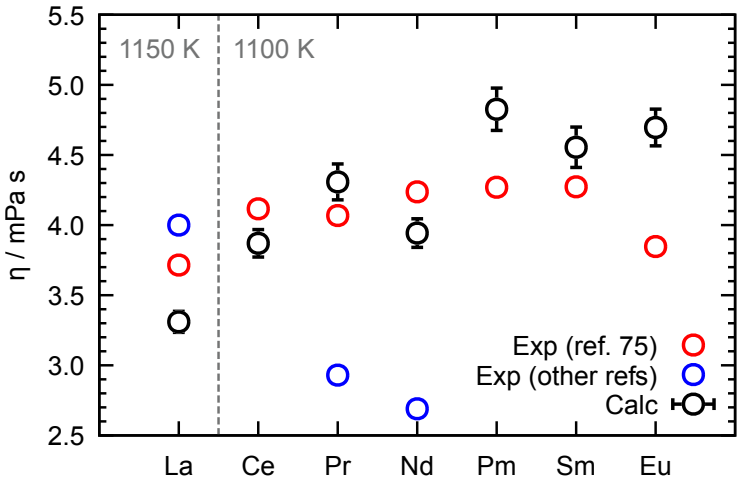

Figure 6: Calculated and experimental[75–77] viscosities of molten MCl_3 salts. The values are given at 1100 K for the Ce−Eu systems and at 1150 K for the La system. The data from ref. 76,77 (blue circles) are extrapolated to the temperatures of interest. The extrapolated value $\eta = 6.2$ mPa s for molten $LaCl_3$ from ref. 64 is not shown.

Diffusion coefficients are much easier to estimate, but, unfortunately, no experimental data are available for comparison for pure MCl_3. The simulated results, given in Figure 7a, show that the values are about $[1.0 - 2.2] \times 10^{-9}$ m^2 s^{-1} and the M^{3+} cations move $1.6 - 1.8$ times slower than the Cl^- anions. This trend is different from the molten alkali metal chlorides, in which cation diffusivities are higher than those of the anion.[29] In our series, the obtained values are the largest for molten $LaCl_3$ because of the higher temperature considered. At constant temperature, the diffusivities slightly decrease from Ce to Nd / Pm and then remain constant up to Eu.

In MCl_3/NaCl systems, lanthanide ions move 2–3 times faster than in neat salt since they no longer form the cation-anion network but behave as isolated ions. The order of magnitude agrees well with the experimental data in NaCl, such as $D(Eu^{3+}) = 2.2 \times 10^{-9}$ m^2 s^{-1}.[78] The

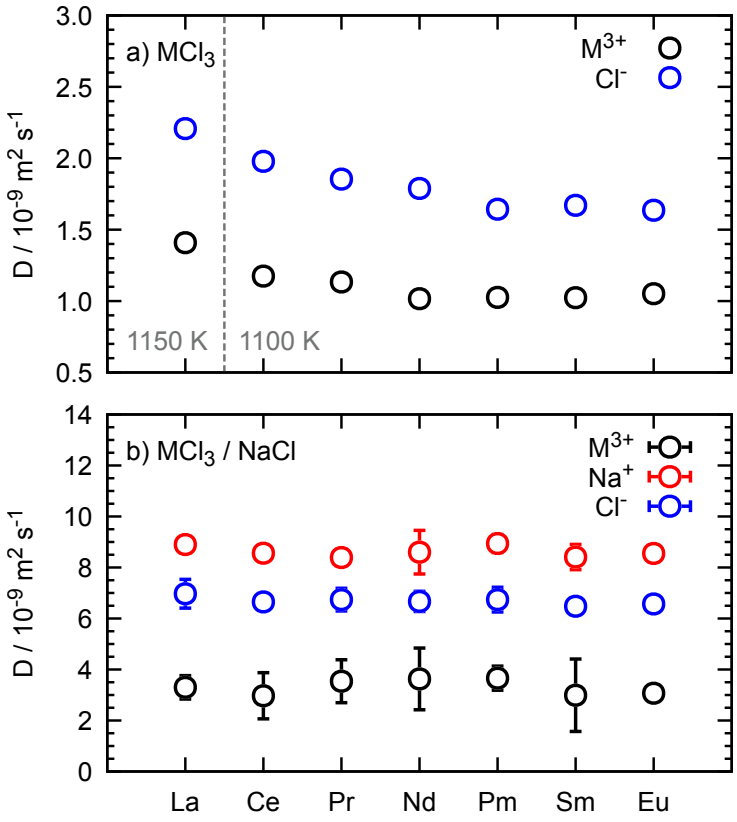

Figure 7: Cation and anion diffusion coefficients in neat MCl_3 salts (a) and MCl_3/NaCl systems (b). The subplot (b) represents the values averaged from three independent trajectories with corresponding standard deviations.

exact trend on how diffusivities change along the series is difficult to identify due to the low concentration and consequently poor statistics. Chloride diffusion coefficients are also notably larger, of about $6.7 \times 10^{-9}\,\mathrm{m^2\,s^{-1}}$, reaching a value close to that in neat NaCl.[79] Sodium cation appears to be the fastest species in the solution, with a diffusivity of about $8.6 \times 10^{-9}\,\mathrm{m^2\,s^{-1}}$.

Conclusions

In conclusion, we developed a general transferable polarisable model for molten lanthanide chlorides and their mixture with sodium chloride, based on a force field fitting procedure and empirical adjustment of dispersion coefficients. Successfully validated, the proposed model provides valuable insight into the local structure and transport properties in the rare-earth series, in particular, giving access to those of poorly studied $PmCl_3$ salt.

Structure analysis showed that the contraction of the ionic radius moderately impacts the $M^{3+}\cdots Cl^-$ interactions in the neat MCl_3 melts so that both the most probable cation-anion separation and the average value of the first shell coordination number decrease along the series. Broad coordination number distributions confirmed a variety of possible metal-chloride complexes, which range from $[MCl_6]^{3-}$ to $[MCl_9]^{6-}$. Such a large number of chloride anions around a single metal ion is only possible when they are shared between neighbouring cations. The $MCl_n^{(n-3)-}$ polyhedra are therefore connected through a corner or an edge, and the corner-sharing becomes dominant with an increase in atomic number from La to Eu.

With the decrease of MCl_3 concentration (to 1 % by molar fraction) in molten NaCl, the average $M^{3+}\cdots Cl^-$ coordination number diminish, and the most probable complexes are $[MCl_6]^{3-}$ to $[MCl_7]^{4-}$. The ratio between complexes strongly depends on the lanthanide ion, being close to one in the case of La^{3+}, and increasing to 4.5 for Eu^{3+}. The M^{3+} cations behave as isolated ions, with a low probability of creating pairs or clusters with short $M^{3+}\cdots M^{3+}$ distances.

By analysing the transport properties, we demonstrated that the lanthanide cations move slower than the chloride anion in neat molten salt. This behaviour is different to what was observed in neat alkali chloride melts, and is related to the increased strength of the cation-anion interaction. In the series, the ionic diffusivities decrease from Ce to Nd / Pm and then do not vary up to Eu. When diluted in NaCl, the M^{3+} diffusion coefficients increase by a factor of 2–3, since they are no longer involved in the lanthanide-chloride network.

The development of those new models bring valuable insight into the structure, chemistry and transport properties of lanthanide chloride salts. This is of particular relevance for the simulation and experiments performed within the nuclear context, such as the simulation of the processes associated to the extraction of lanthanides during the reprocessing of spent chloride salts, or the use of lanthanide-based salts as simulants while developing and operating experimental facilities.

Acknowledgement

This work was performed as part of the ISAC (Innovative System for Actinide Conversion) project funded by the France 2030 government program. The simulations were performed on the SACADO MeSU platform at Sorbonne Université and using HPC resources from GENCI [CINES/IDRIS/TGCC/IRENE)] under the allocations 2024-A0160906008 and 2024-A0150906922.

Data availability

Examples of input files used for the MD simulations are available in the Zenodo repository with the identifier 10.5281/zenodo.14212261.

References

(1) Locatelli, G.; Mancini, M.; Todeschini, N. Generation IV nuclear reactors: Current status and future prospects. *Energy Policy* **2013**, *61*, 1503–1520.

(2) Mausolff, Z.; DeHart, M.; Goluoglu, S. Design and assessment of a molten chloride fast reactor. *Nucl. Eng. Des.* **2021**, *379*, 111181.

(3) Ho, A.; Memmott, M.; Hedengren, J.; Powell, K. M. Exploring the benefits of molten salt reactors: An analysis of flexibility and safety features using dynamic simulation. *Digit. Chemi. Eng.* **2023**, *7*, 100091.

(4) Roper, R.; Harkema, M.; Sabharwall, P.; Riddle, C.; Chisholm, B.; Day, B.; Marotta, P. Molten salt for advanced energy applications: A review. *Ann. Nucl. Energy* **2022**, *169*, 108924.

(5) Yin, T.-q.; Xue, Y.; Yan, Y.-d.; Ma, Z.-c.; Ma, F.-q.; Zhang, M.-l.; Wang, G.-l.; Qiu, M. Recovery and separation of rare earth elements by molten salt electrolysis. *Int. J. Miner. Metall. Mater.* **2021**, *28*, 899–914.

(6) Galashev, A. Y. Recovery of actinides and fission products from spent nuclear fuel via electrolytic reduction: Thematic overview. *Int. J. Energy Res.* **2022**, *46*, 3891–3905.

(7) Serp, J.; Allibert, M.; Beneš, O.; Delpech, S.; Feynberg, O.; Ghetta, V.; Heuer, D.; Holcomb, D.; Ignatiev, V.; Kloosterman, J. L. *et al.* The molten salt reactor (MSR) in generation IV: overview and perspectives. *Progress in Nuclear Energy* **2014**, *77*, 308–319.

(8) Rollet, A.-L.; Salanne, M. Studies of the local structures of molten metal halides. *Annual Reports Section "C" (Physical Chemistry)* **2011**, *107*, 88–123.

(9) Zamoryanskaya, M. V.; Burakov, B. E. Feasibility Limits in Using Cerium as a Surro-

gate for Plutonium Incorporation in Zircon, Zirconia and Pyrochlore. *Mater. Res. Soc. Symp. Proc.* **2000**, *663*, 301.

(10) Feuchter, H.; Duval, S.; Volkringer, C.; Ouf, F.-X.; Rigollet, L.; Cantrel, L.; De Mendonca Andrade, M.; Salm, F.; Lavalette, C.; Loiseau, T. Influence of Light and Temperature on the Extractability of Cerium(IV) as a Surrogate of Plutonium(IV) and its Effect on the Simulation of an Accidental Fire in the PUREX Process. *ACS Omega* **2019**, *4*, 12896–12904.

(11) Pelton, A. D.; Chartrand, P. Thermodynamic evaluation and optimization of the LiCl-NaCl-KCl-RbCl-CsCl-MgCl2-CaCl2 system using the modified quasi-chemical model. *Metall. Mater. Trans. A* **2001**, *32*, 1361–1383.

(12) Ard, J. C.; Schorne-Pinto, J.; Aziziha, M.; Yingling, J. A.; Mofrad, A. M.; Johnson, K. E.; Dixon, C. M.; Besmann, T. M. Thermodynamic assessments or reassessments of 30 pseudo-binary and -ternary salt systems. *J. Chem. Thermodyn.* **2023**, *177*, 106931.

(13) Duvail, M.; Spezia, R.; Vitorge, P. A Dynamic Model to Explain Hydration Behaviour along the Lanthanide Series. *ChemPhysChem* **2008**, *9*, 693–696.

(14) Duvail, M.; Vitorge, P.; Spezia, R. Building a polarizable pair interaction potential for lanthanoids(III) in liquid water: A molecular dynamics study of structure and dynamics of the whole series. *J. Chem. Phys.* **2009**, *130*, 104501.

(15) D'Angelo, P.; Spezia, R. Hydration of Lanthanoids(III) and Actinoids(III): An Experimental/Theoretical Saga. *Chem. Eur. J.* **2012**, *18*, 11162–11178.

(16) D'Angelo, P.; Migliorati, V.; Spezia, R.; De Panfilis, S.; Persson, I.; Zitolo, A. K-edge XANES investigation of octakis(DMSO)lanthanoid(iii) complexes in DMSO solution and solid iodides. *Phys. Chem. Chem. Phys.* **2013**, *15*, 8684–8691.

(17) Bodo, E.; Macaluso, V.; Spezia, R. Solvent Structure around Lanthanoid(III) Ions in Liquid DMSO As Revealed by Polarizable Molecular Dynamics Simulations. *J. Phys. Chem. B* **2015**, *119*, 13347–13357.

(18) Mochinaga, J.; Ikeda, M.; Igarashi, K.; Fukushima, K.; Iwadate, Y. X-ray diffraction and Raman spectroscopic study on the short-range structure of molten CeCl3. *J. Alloys Compd.* **1993**, *193*, 36–37.

(19) Iwadate, Y.; Okako, N.; Koyama, Y.; Kubo, H.; Fukushima, K. In *Melting behaviour in hexagonal CeCl3 and monoclinic ErCl3 crystals*; Nomura, H., Kawaizumi, F., Yarwood, J., Eds.; Elsevier, 1995; Vol. 83; pp 369–372.

(20) Emerson, M. S.; Sharma, S.; Roy, S.; Bryantsev, V. S.; Ivanov, A. S.; Gakhar, R.; Woods, M. E.; Gallington, L. C.; Dai, S.; Maltsev, D. S. *et al.* Complete Description of the LaCl3–NaCl Melt Structure and the Concept of a Spacer Salt That Causes Structural Heterogeneity. *J. Am. Chem. Soc.* **2022**, *144*, 21751–21762.

(21) Glover, W. J.; Madden, P. A. Raman spectra of ionic liquids: A simulation study of LaCl3 and its mixtures with alkali chlorides. *J. Chem. Phys.* **2004**, *121*, 7293–7303.

(22) Madden, P. A.; Wilson, M.; Hutchinson, F. Raman spectra of ionic liquids: Interpretation via computer simulation. *J. Chem. Phys.* **2004**, *120*, 6609–6620.

(23) Okamoto, Y.; Shiwaku, H.; Yaita, T.; Narita, H.; Tanida, H. Local structure of molten LaCl3 by K-absorption edge XAFS. *J. Mol. Struct.* **2002**, *641*, 71–76.

(24) Okamoto, Y.; Suzuki, S.; Shiwaku, H.; Ikeda-Ohno, A.; Yaita, T.; Madden, P. A. Local Coordination about La3+ in Molten LaCl3 and Its Mixtures with Alkali Chlorides. *J. Phys. Chem. A* **2010**, *114*, 4664–4671.

(25) Okamoto, Y.; Madden, P. A. Structural study of molten lanthanum halides by X-ray

diffraction and computer simulation techniques. *J. Phys. Chem. Solids* **2005**, *66*, 448–451.

(26) Madden, P. A.; Heaton, R.; Aguado, A.; Jahn, S. From first-principles to material properties. *J. Mol. Struct.: THEOCHEM* **2006**, *771*, 9–18.

(27) Madden, P. A.; Wilson, M. 'Covalent'effects in 'ionic'systems. *Chem. Soc. Rev* **1996**, *25*, 339–350.

(28) Salanne, M.; Madden, P. A. Polarization effects in ionic solids and melts. *Mol. Phys.* **2011**, *109*, 2299–2315.

(29) Ishii, Y.; Kasai, S.; Salanne, M.; Ohtori, N. Transport coefficients and the Stokes–Einstein relation in molten alkali halides with polarisable ion model. *Mol. Phys.* **2015**, *113*, 2442–2450.

(30) Ishii, Y.; Kiko, S.; Ohtori, N. Analysis of the Transport Properties of Alkaline-earth Halides MX_2 (M = Ca, Sr, Ba, and X = F, Cl, Br) by Simulation with a Polarizable Ion Model. *Electrochemistry* **2024**, *92*, 043024.

(31) Salanne, M.; Simon, C.; Turq, P.; Madden, P. A. Calculation of Activities of Ions in Molten Salts with Potential Application to the Pyroprocessing of Nuclear Waste. *J. Phys. Chem. B* **2008**, *112*, 1177–1183.

(32) Corradini, D.; Madden, P. A.; Salanne, M. Coordination numbers and physical properties in molten salts and their mixtures. *Faraday Discussions* **2016**, *190*, 471–486.

(33) Jiang, T.; Wang, N.; Cheng, C.-M.; Peng, S.-M.; Liu-Ming, Y. Molecular Dynamics Simulation on the Structure and Thermodynamics of Molten LiCl-KCl-$CeCl_3$. *Acta Phys. -Chim. Sin.* **2016**, *32*, 647–655.

(34) Matsumiya, M.; Takagi, R. A Molecular Dynamics Simulation of the Electric and Thermodynamic Properties in Molten (Nd1/3, Na or K)Cl Mixtures. *Z. fur Naturforsch. A* **2001**, *56*, 466–472.

(35) Iwadate, Y.; Yamoto, H.; Fukushima, K.; Takagi, R. Molecular dynamics study of ionic aggregation in molten SmCl3-NaCl system. *J. Mol. Liq.* **1999**, *83*, 41–49.

(36) Fuller, J.; Moon, J.; Zhang, J.; Chidambaram, D.; An, Q. Coordination and thermophysical properties of select trivalent lanthanides in LiCl–KCl. *Phys. Chem. Chem. Phys.* **2022**, *24*, 13102–13109.

(37) Moon, J.; Fuller, J.; An, Q.; Chidambaram, D. Temperature and anion ligand field dependence of LnCl3 (Ln = Nd, Dy, Sm) electronic absorption spectra in LiCl–KCl eutectic molten salt. *Prog. Nuclear Energy* **2023**, *157*, 104584.

(38) Tang, K. T.; Peter Toennies, J. An improved simple model for the van der Waals potential based on universal damping functions for the dispersion coefficients. *J. Chem. Phys.* **1984**, *80*, 3726–3741.

(39) Hutter, J.; Iannuzzi, M.; Schiffmann, F.; VandeVondele, J. cp2k: atomistic simulations of condensed matter systems. *Wiley Interdiscip. Rev. Comput. Mol.* **2014**, *4*, 15–25.

(40) VandeVondele, J.; Krack, M.; Mohamed, F.; Parrinello, M.; Chassaing, T.; Hutter, J. Quickstep: Fast and accurate density functional calculations using a mixed Gaussian and plane waves approach. *Comput. Phys. Commun.* **2005**, *167*, 103–128.

(41) Lu, J.-B.; Cantu, D. C.; Nguyen, M.-T.; Li, J.; Glezakou, V.-A.; Rousseau, R. Norm-Conserving Pseudopotentials and Basis Sets To Explore Lanthanide Chemistry in Complex Environments. *J. Chem. Theory Comput.* **2019**, *15*, 5987–5997.

(42) Perdew, J. P.; Burke, K.; Ernzerhof, M. Generalized Gradient Approximation Made Simple. *Phys. Rev. Lett.* **1996**, *77*, 3865–3868.

(43) Iwadate, Y. In *Chapter 260 - Structures and Properties of Rare-Earth Molten Salts*; Bünzli, J.-C. G., Pecharsky, V. K., Eds.; Elsevier, 2014; Vol. 44; pp 87–168.

(44) Cheisson, T.; Schelter, E. J. Rare earth elements: Mendeleev's bane, modern marvels. *Science* **2019**, *363*, 489–493.

(45) Marin-Laflèche, A.; Haefele, M.; Scalfi, L.; Coretti, A.; Dufils, T.; Jeanmairet, G.; Reed, S.; Serva, A.; Berthin, R.; Bacon, C. *et al.* MetalWalls: A Classical Molecular Dynamics Software Dedicated to the Simulation of Electrochemical Systems. *J. Open Source Softw.* **2020**, *5*, 2373.

(46) Coretti, A.; Bacon, C.; Berthin, R.; Serva, A.; Scalfi, L.; Chubak, I.; Goloviznina, K.; Haefele, M.; Marin-Laflèche, A.; Rotenberg, B. *et al.* MetalWalls: Simulating electrochemical interfaces between polarizable electrolytes and metallic electrodes. *J. Chem. Phys.* **2022**, *157*, 184801.

(47) Martínez, L.; Andrade, R.; Birgin, E. G.; Martínez, J. M. PACKMOL: A package for building initial configurations for molecular dynamics simulations. *J. Comp. Chem.* **2009**, *30*, 2157–2164.

(48) Brehm, M.; Kirchner, B. TRAVIS - A Free Analyzer and Visualizer for Monte Carlo and Molecular Dynamics Trajectories. *J. Chem. Inf. Model.* **2011**, *51*, 2007–2023.

(49) Brehm, M.; Thomas, M.; Gehrke, S.; Kirchner, B. TRAVIS—A free analyzer for trajectories from molecular simulation. *J. Chem. Phys.* **2020**, *152*, 164105.

(50) Ercole, L.; Marcolongo, A.; Baroni, S. Accurate thermal conductivities from optimally short molecular dynamics simulations. *Sci. Rep.* **2017**, *7*, 15835.

(51) Ercole, L.; Bertossa, R.; Bisacchi, S.; Baroni, S. SporTran: A code to estimate transport coefficients from the cepstral analysis of (multivariate) current time series. *Comput. Phys. Commun.* **2022**, *280*, 108470.

(52) Yeh, I.-C.; Hummer, G. System-Size Dependence of Diffusion Coefficients and Viscosities from Molecular Dynamics Simulations with Periodic Boundary Conditions. *J. Phys. Chem. B* **2004**, *108*, 15873–15879.

(53) Maginn, E.; Messerly, R.; Carlson, D.; Roe, D.; Elliott, J. Best Practices for Computing Transport Properties 1. Self-Diffusivity and Viscosity from Equilibrium Molecular Dynamics [Article v1.0]. *Living J. Comp. Mol. Sci.* **2018**, *1*.

(54) Janz, G. J.; Tomkins, R. P. T.; Allen, C. B.; Downey, J., J. R.; Garner, G. L.; Krebs, U.; Singer, S. K. Molten salts: Volume 4, part 2, chlorides and mixtures—electrical conductance, density, viscosity, and surface tension data. *J. Phys. Chem. Ref. Data* **1975**, *4*, 871–1178.

(55) Salanne, M.; Simon, C.; Turq, P.; Madden, P. A. Simulation of the liquid–vapor interface of molten LiBeF3. *C. R. Chim.* **2007**, *10*, 1131–1136.

(56) Irving, J. H.; Kirkwood, J. G. The Statistical Mechanical Theory of Transport Processes. IV. The Equations of Hydrodynamics. *J. Chem. Phys.* **1950**, *18*, 817–829.

(57) Ghoufi, A.; Malfreyt, P.; Tildesley, D. J. Computer modelling of the surface tension of the gas–liquid and liquid–liquid interface. *Chem. Soc. Rev.* **2016**, *45*, 1387–1409.

(58) Yan, D.; Ro, S.; Sunam, O.; Kim, S. On the Global Rare Earth Elements Utilization and Its Supply-Demand in the Future. *IOP Conf. Ser.: Earth Environ. Sci.* **2020**, *508*, 012084.

(59) Rycerz, L.; Gaune-Escard, M. Thermodynamics of EuCl3: Experimental Enthalpy of Fusion and Heat Capacity and Estimation of Thermodynamic Functions up to 1300 K. *Z. Naturforsch. A* **2002**, *57*, 215–220.

(60) Gaune-Escard, M.; Bogacz, A.; Rycerz, L.; Szczepaniak, W. Heat capacity of LaCl3, CeCl3, PrCl3, NdCl3, GdCl3, DyCl3. *J. Alloys Compd.* **1996**, *235*, 176–181.

(61) Marcus, Y. In *Heat Capacities of Molten Salts*; Wilhelm, E., Letcher, T. M., Eds.; The Royal Society of Chemistry, 2010; pp 472–489.

(62) Igarashi, K. Molar Volume and Surface Tension of Molten LaCl3-KCl Mixtures. *Z. Naturforsch. A* **1987**, *42*, 690–694.

(63) Shishalov, V. I.; Kovalevskii, A. V. The properties of the surface of molten mixtures of the LiCl-KCl eutectic with praseodymium, samarium, erbium, and ytterbium chlorides. *Russ. J. Phys. Chem. A* **2011**, *85*, 108–111.

(64) Janz, G. J. *Thermodynamic and transport properties for molten salts : correlation equations for critically evaluated density, surface tension, electrical conductance, and viscosity data*; American Chemical Society and the American Institute of Physics, 1988; p 309.

(65) Lu, G.; He, M.; Kang, Z. Study on surface tension and surface phase of molten MCl-CeCl3 (M = Li, Na, K, Cs): A comparison of Butler's equation and a newly-proposed model. *Fluid Ph. Equilib.* **2016**, *427*, 345–352.

(66) Mochinaga, J.; Iwadate, Y.; Fukushima, K. Short Range Structures of Several Rare Earth Chloride Melts. *Mater. Sci. Forum* **1991**, *73-75*, 147–152.

(67) Wasse, J. C.; Salmon, P. S. Structure of molten lanthanum and cerium tri-halides by the method of isomorphic substitution in neutron diffraction. *J. Condens. Matter Phys.* **1999**, *11*, 1381.

(68) Matsuura, H.; Watanabe, S.; Sakamoto, T.; Kanuma, T.; Naoi, K.; Hatcho, M.; Kitamura, N.; Akatsuka, H.; Adya, A. K.; Honma, T. *et al.* Short-range structure of molten CeCl3 and NdCl3 determined by XAFS. *J. Alloys Compd.* **2006**, *408-412*, 80–83.

(69) Li, B.; Jones, Z. R.; Eiroa-Lledo, C.; Knope, K. E.; Mocko, V.; Stein, B. W.;

Wacker, J. N.; Kozimor, S. A.; Batista, E. R.; Yang, P. Structure and Dynamics of NaCl/KCl/CaCl2–EuCln (n = 2, 3) Molten Salts. *Inorg. Chem.* **2023**, *62*, 10528–10538.

(70) Hutchinson, F.; Rowley, A. J.; Walters, M. K.; Wilson, M.; Madden, P. A.; Wasse, J. C.; Salmon, P. S. Structure of molten MCl3 systems from a polarizable ion simulation model. *J. Chem. Phys.* **1999**, *111*, 2028–2037.

(71) Bruno, J.; Ewing, R. C. Spent Nuclear Fuel. *Elements* **2006**, *2*, 343–349.

(72) Emerson, M. S.; Ivanov, A. S.; Gallington, L. C.; Maltsev, D. S.; Halstenberg, P.; Dai, S.; Roy, S.; Bryantsev, V. S.; Margulis, C. J. Heterogeneous Structure, Mechanisms of Counterion Exchange, and the Spacer Salt Effect in Complex Molten Salt Mixtures Including LaCl3. *J. Phys. Chem. B* **2024**, *128*, 3972–3980.

(73) Okamoto, Y.; Hayashi, H.; Ogawa, T. X-Ray Diffraction Analysis of Molten Trivalent Halides. *Jpn. J. Appl. Phys.* **1999**, *38*, 156.

(74) Pastore, G.; Tatlipinar, H.; Tosi, M. P. Local Coordination and Medium Range Order in Molten Trivalent Metal Chlorides: The Role of Screening by the Chlorine Component. *Phys. Chem. Liq.* **1996**, *31*, 189–200.

(75) Potapov, A.; Sato, Y. Viscosity of Molten Rare Earth Metal Trichlorides II. Cerium Subgroup. *Z. Naturforsch. A* **2011**, *66*, 649–655.

(76) Cho, K.; Kuroda, T. Viscosity of four molten rare-earth chlorides: PrCl3, NdCl3, GdCl3, and DyCl3. *Denki Kagaku oyobi Kogyo Butsuri Kagaku* **1972**, *40*, 878.

(77) Hayashi, H.; Okamoto, Y.; Ogawa, T.; Sato, Y. Viscosity of Molten Rare Earth Trichlorides. Molten salt chemistry and technology. 1998; pp 257–260.

(78) Li, X.; Zhang, Y.; Yue, B.; Yan, L.; Jiang, T.; Peng, S. Unifying the diffusion coefficients of lanthanides and actinides in binary molten salt mixtures: A data review. *J. Mol. Liq.* **2020**, *297*, 112106.

(79) Bockris, J. O.; Hooper, G. W. Self-diffusion in molten alkali halides. *Discuss. Faraday Soc.* **1961**, *32*, 218–236.

Table 2: Born-Mayer potential parameters. The Tang-Toennies damping parameters for dispersion interactions were equal $b_6^{ij} = 1.5$ and $b_8^{ij} = 1.0$ for ion pairs involving M^{3+} ions, and $b_6^{ij} = b_8^{ij} = 1.7$ for the opposite case. The values for Na^+ and Cl^- interactions were taken from reference 29.

Ion pair		B^{ij}	α^{ij}	C_6^{ij}	C_8^{ij}
Cl^-	Cl^-	275.100	1.797	140.000	280.000
Na^+	Na^+	0.000	5.000	11.700	51.800
La^{3+}	La^{3+}	0.000	3.000	47.700	100.000
Ce^{3+}	Ce^{3+}	0.000	3.000	44.470	93.229
Pr^{3+}	Pr^{3+}	0.000	3.000	44.000	92.243
Nd^{3+}	Nd^{3+}	0.000	3.000	37.386	78.378
Pm^{3+}	Pm^{3+}	0.000	3.000	35.449	74.317
Sm^{3+}	Sm^{3+}	0.000	3.000	34.624	72.587
Eu^{3+}	Eu^{3+}	0.000	3.000	32.916	69.006
Cl^-	Na^+	67.500	1.726	47.400	187.300
Cl^-	La^{3+}	392.395	1.800	81.719	167.332
Cl^-	Ce^{3+}	363.903	1.800	78.904	161.568
Cl^-	Pr^{3+}	345.661	1.800	78.485	160.711
Cl^-	Nd^{3+}	328.953	1.800	72.347	148.141
Cl^-	Pm^{3+}	311.280	1.800	70.448	144.252
Cl^-	Sm^{3+}	297.938	1.800	69.623	142.564
Cl^-	Eu^{3+}	283.520	1.800	67.884	139.002
Na^+	La^{3+}	0.000	5.000	23.624	71.972
Na^+	Ce^{3+}	0.000	5.000	22.810	69.493
Na^+	Pr^{3+}	0.000	5.000	22.689	69.124
Na^+	Nd^{3+}	0.000	5.000	20.914	63.718
Na^+	Pm^{3+}	0.000	5.000	20.365	62.045
Na^+	Sm^{3+}	0.000	5.000	20.127	61.319
Na^+	Eu^{3+}	0.000	5.000	19.624	59.787

All the values are given in atomic units.

Table 3: Tang-Toennies damping parameters for charge-dipole interactions, where the first atom has a partial charge, and the second an induced dipole. The values for Na^+ and Cl^- pairs were taken from reference 29.

Ion	b_4^{ij}	c_4^{ij}
$M^{3+}\cdots Cl^-$	1.250	1.000
$Na^+\cdots Cl^-$	1.760	3.000
$Cl^-\cdots M^{3+}$	1.250	−1.000
$Cl^-\cdots Na^+$	1.760	0.697

All the values are given in atomic units.